AIAA JOURNAL
Vol. 32, No. 3, March 1994

Active Plate and Missile Wing Development Using Directionally Attached Piezoelectric Elements

Ron Barrett*
University of Kansas, Lawrence, Kansas 60045

The properties of directionally attached piezoelectric (DAP) elements and a low aspect ratio DAP torque-plate wing are investigated. Tests show that isotropic piezoceramic elements exhibit orthotropic behavior when directionally attached using any of three methods: 1) partial attachment, 2) transverse shear lag, and 3) differential stiffness bonding. Closed-form expressions of DAP strains based on laminated plate theory are presented. The models demonstrate that DAP elements can generate pure extension, bending, or twist deflections in beams and plates. Activation sequences and balancing strains for DAP and conventionally attached piezoelectric (CAP) elements based on laminated plate theory are presented. Experimental beam specimens were constructed to verify the models. Tests show that 0.030-in. (0.0762-cm) thick aluminum beams with antisymmetrically laminated DAP elements produce twist rates of 0.23 deg/in. (9 deg/m) and bending rates in excess of 0.36 deg/in. (14 deg/m) with theory and experiment in close agreement. A DAP torque-plate was constructed of 8.0-mil-thick piezoceramic elements bonded antisymmetrically on a 5-mil steel substrate. The torque plate was then used to induce pitch deflections in a subsonic missile fin with a NACA 0012 profile and an aspect ratio of 1.4. The wing demonstrated a break frequency in excess of 80 Hz and static pitch deflections of 8.5 deg, showing excellent correlation with theory.

Nomenclature

A, B, D	= extensional coupling, and bending stiffness matrices
d_{15}	= piezoelectric in-plane to in-plane shear-charge coefficient
d_{31}	= piezoelectric through thickness to longitudinal extension-charge coefficient
d_{32}	= piezoelectric through thickness to lateral extension-charge coefficient
d_{35}	= piezoelectric through thickness to in-plane shear-charge coefficient
d_{36}	= piezoelectric through thickness to twist-charge coefficient
E	= modulus of elasticity
E_3	= through-thickness acuation potential
L	= length of DAP element
OR	= orthotropy ratio, $E_{L\text{eff}}/E_{T\text{eff}}$
t	= thickness
u, v, w	= elemental deflections in the x, y, z directions
W	= width of DAP element
α	= angle of attack
ϵ	= in-plane strain
Θ	= ply orientation angle
κ	= plate curvature
Λ	= free piezoelectric element active strain
λ	= balancing strain of CAP elements
ν	= Poisson's ratio

Subscripts

a	= actuator
an	= antisymmetric
b	= bond layer
C	= CAP actuator ply
D	= DAP actuator ply
eff	= effective (due to combined attachment methods)
eff$o$	= original effective (due to attachment geometry)
l	= laminate
o	= original (without any attachment effects)
s	= substrate
sy	= symmetric
1, 2, 3	= longitudinal, lateral, and through-thickness directions
5	= in-plane shear
6	= twist

Received April 16, 1992; revision received June 16, 1992; accepted for publication July 28, 1992.

*Graduate Fellow; currently Assistant Professor, Aerospace Engineering Department, Auburn University, Auburn, AL 36849.

Introduction

ADAPTIVE structures that are capable of inducing bending and extension deflections have been investigated and successfully modeled by numerous experimenters. Crawley and Anderson,[1] Anderson,[2] and Hanagud et al.[3] are just a few of the technologists who have modeled active plates in bending and extension. Improvements to the Euler beam and laminated plate theory models have added to the prediction capability. Most of these efforts have been centered on capturing the fundamental physics of active structures that use isotropic actuator elements like lead zirconate titanate (PZT). Crawley and De Luis[4] included shear lag in their dynamic performance estimations of active beams using piezoceramic actuator elements. They estimated the reductions in stress due to shear lag in isotropic actuator elements in bending and extension. To control structures with masses placed off the elastic axis or in twist modes, direct manipulation of the structural twist is necessary. To achieve direct twist control, actuator elements that are shear active, twist active, inherently orthotropic or that exhibit unequal active strains longitudinally and laterally are needed. Until recently, no investigator has used active twist control because no suitable shear-capable or twist-capable piezoceramic elements (possessing a d_{35} or d_{36} property) have been available. For PZT, a small amount of shear actuation is available through the d_{15} property. Sung et al.[5] used d_{15} to actuate rods in torsion. They showed that circumferentially charged PZT tubes produce twist deflections that can be used to control torsional vibrations. Unfortunately, using in-plane charges in plates has proved difficult as extremely high voltages are required and the substrates are often conductive and sink current around the elements. Accordingly, most investigators have used a simple method of applying a charge

through the thickness of the element. Lee[6] successfully demonstrated that polyvinylidene fluoride (PVDF) can be arranged on substrates antisymmetrically and charged through the thickness to produce twist deflections. This breakthrough was possible because PVDF generates in-plane strains that are greater in the longitudinal direction than the transverse direction. Unfortunately, piezoelectric polymers like PVDF have an extremely low modulus (0.29 Msi) and require extremely high voltages for actuation.

Several other experimenters have worked around these twist-induction problems by applying PZT elements to coupled substrates. Crawley and Lazarus[7] worked on twist manipulation with extension-twist and bending-twist coupled plates. The plates were bent or extended by the PZT elements to induce twist deflections. Small but significant deflections were generated. Crawley et al.[8] took this investigation one step further when they used cantilevered coupled plates as lifting surfaces. This first investigation into the new field of active aeroservoelasticity showed that air loads could be used to effectively magnify small twist deflections. As their bending-twist coupled plates were bent, twist resulted that increased the airloads that, in turn, increased the twist. Unfortunately, the high degree of coupling necessary to produce these deflections meant that any wing that used this method could not be optimized for strength and would eventually suffer from forms of divergence.

To get around the divergence problems of using structural coupling to increase plate deflections, investigators sought a method of using uncoupled substrates with stiff actuator elements like PZT. Barrett[9-12] and Chen et al.[13] showed that isotropic PZT elements could be given orthotropic characteristics through directional attachment. These directionally attached piezoelectric (DAP) elements were laminated at off-axis angles to generate torsional shear flows. DAP elements were used to twist uncoupled plates and aerodynamic surfaces with significantly higher deflections than those generated by other materials (like PVDF). The DAP elements were laminated in rotor blades, demonstrating that air loads could be significantly manipulated and used for vibration reduction as shown by Nitzsche and Breitbach.[14] Experimentation by Barrett[9,11] showed that the DAP elements could also be used to produce twist deflections in wings. Barrett showed that 1.4-deg twist deflections could be generated in an aspect ratio 5, NACA 0012 wing. This small amount of twist deflection was sufficient for some forms of flight control, but higher deflections are required for high-performance flight vehicles. To achieve the higher deflections, the thickness of the wing would have to be reduced to the point at which it could no longer carry the required bending loads. Accordingly, a new design using a thin active torque plate that generates very high torsional deflections was conceived. This torque plate is strengthened in bending by a spar and placed at the quarter-chord within an aerodynamic shell. Twist deflections of the plate induce pitch deflections of the wing shell which is free to rotate about the spar at the wing root. This investigation is centered on analyzing the fundamental structural aspects of this design and demonstrating that large pitch deflections may be generated by such a solid state fin design.

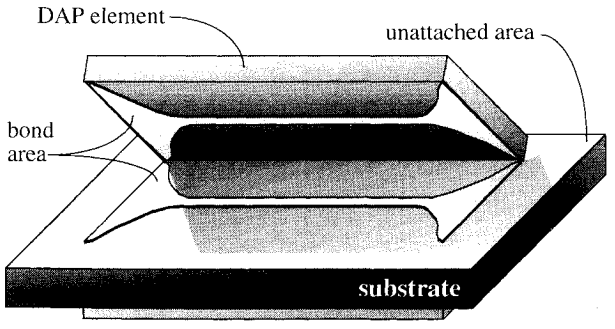

Fig. 1 Directional attachment through partial attachment.

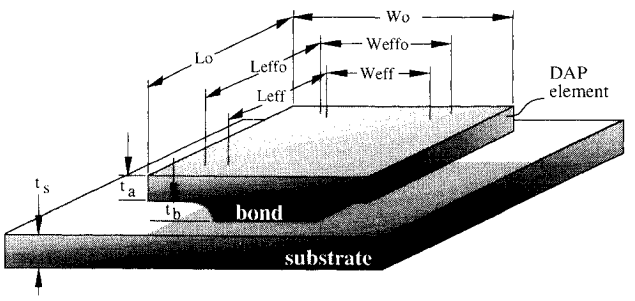

Fig. 2 DAP attachment schematic.

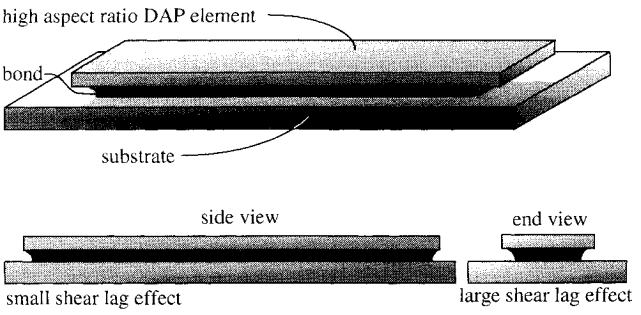

Fig. 3 Directional attachment through transverse shear lag.

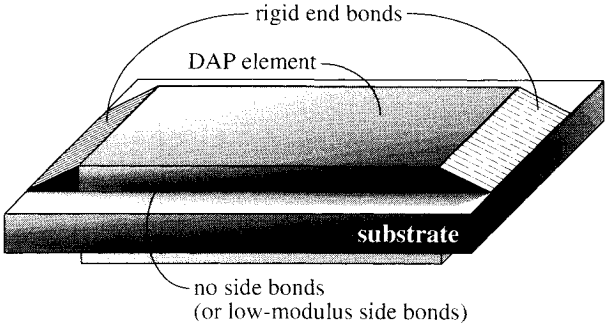

Fig. 4 Directional attachment through differential stiffness bonding.

Analysis of DAP Elements

There are two steps in the modeling of DAP elements. The first is to establish the effective stiffnesses of the element in each DAP ply. The second step is to use these effective stiffnesses in plate models so that the behavior of the laminate can be predicted.

Modeling Directional Attachment

There are three methods of achieving directional attachment: 1) partial attachment, 2) transverse shear lag, and 3) differential stiffness bonding. Each method is used for a slightly different purpose, and each tends to enhance the performance of the other methods. Figures 1-4 outline the fundamentals of each attachment technique and show the overall schematic of directional attachment. In practice, all three methods of directional attachment are used simultaneously for best results. Each method provides the DAP element with increasing orthotropy (which increases the amount of twist deflection) and allows the element to perform with minimal warping and high resistance to debonds.

Directional attachment through partial attachment gives the DAP element a high degree of orthotropy and is amenable to surface lamination and embedding. Figure 1 shows that the

DAP element is bonded rigidly to the substrate in the longitudinal direction. In the transverse direction, the sides of the DAP element are more free to expand and contract; accordingly, they do little work on the substrate in the transverse direction. In early stages of experimentation, stress concentrations at the ends of the rectangular attachment areas caused frequent debonds.[9] Differential stiffness bonding and bondline tailoring into modified "I" patterns or inverted ellipses have eliminated the debond problem.

The models of directional attachment through partial attachment take into account the geometry of the bond. The models adjust the effective longitudinal and lateral stiffnesses of the element and assume that the bonding strip extends the complete length of the element and only part of the width of the element. These new stiffness modification models, Eqs. (1) and (2), improve on earlier models that could only account for rectangular attachment areas[9-11]:

$$E_{L\text{eff}o} = E_{Lo}\left[\frac{L_{\text{eff}o}}{L_o} - \frac{(W_o - W_{\text{eff}o})^2}{2L_oW_o}\right] \tag{1}$$

$$E_{T\text{eff}o} = E_{To}\int_0^{Lo} \frac{W_{\text{eff}o}(x)}{W_oL_o}\,dx \tag{2}$$

The original effective transverse and longitudinal stiffnesses of the DAP actuator ply are modified by the geometry of the element to account for the partial attachment. Figure 2 shows the arrangement of the original, original effective, and effective dimensions of a DAP element. Partial attachment is normally carried out in the transverse direction so as to reduce the transverse stiffness, but the longitudinal direction may also experience some partial attachment from the manufacturing process and is accordingly accounted for through the $L_{\text{eff}o}/L_o$ term.

The second method of achieving directional attachment is through transverse shear lag. Shear lag reduces the effective transverse stiffness of the DAP element by allowing it to strain laterally with little restriction as shown in Fig. 3. High orthotropies from transverse shear lag are most common on elements with high aspect ratios. However, some difference in stiffness through transverse shear lag will occur in all elements with aspect ratios other than 1.

Longitudinally, the shear lag is minimal with respect to the total element length, and the longitudinal strain transmission to the substrate is maintained. As with partial attachment, transverse shear lag is dependent on element geometry and attachment area geometry. Transverse shear lag is also a function of the thickness and stiffness of bond material. It is seen that the higher the elemental aspect ratio, the greater the orthotropy. Equation (3) shows that the original effective modulus $E_{L\text{eff}o}$ can be modified to obtain the effective modulus by selecting the location on the DAP element where the element stress reaches 50% of the midplane stress:

$$\frac{E_{L\text{eff}}}{E_{L\text{eff}o}} = \frac{\sinh^{-1}\{(\sinh/2)[(L_{\text{eff}o}/2)\sqrt{(G_b/t_at_bE_a)}]\}}{(L_{\text{eff}o}/2)\sqrt{(G_b/t_at_bE_a)}} \tag{3}$$

The effective transverse stiffness is obtained by substituting the original effective widths for lengths in Eq. (3). The effective shear modulus $G_{LT\text{eff}}$ of the DAP element is obtained by using similar procedures.

Directional attachment through differential stiffness bonding is more difficult to model as the end and side fixities are dependent on many variables and the relationships become nonlinear. In general, the purpose of end bonding has been to reduce the stress concentrations in the shear attachment and to aid in preventing arcing at the lead locations as seen in Fig. 4.

End bonding is shown to make the DAP element more resistant to debonds. End bonding alone is not normally used because the elements easily warp and buckle when in compression with only end bonds. When in tension, the elements tend to fail at the bond juncture. End bonding works well when used with partial attachment since the element is attached strongly in shear and prevented from buckling. The net effect of stiff end bonding is to increase the orthotropy of the element so that $E_{L\text{eff}}/E_{Lo} \cong L_{\text{eff}o}/L_o \cong 1$.

Plate Theory Models

Classical laminated plate theory (CLPT) is used to model conventionally attached piezoceramic (CAP) and DAP elements. CAP elements have been used by most investigators because of the ease of manufacture and analysis. The CLPT analysis and formulation follow the normal laminated plate theory assumptions laid out by Jones.[15] The elements may be surface bonded or embedded in the structure in any sequence, actuated in extension or contraction, and oriented at any angle. The in-plane strain components are assumed constant through the thickness and the strains caused by bending are assumed to be linearly varying through the thickness of the plate.

The formulation that Jones[15] used for modeling thermally induced strains in lamina can be modified to account for active strains induced by the DAP and CAP elements. The laminate shape is cast in terms of the in-plane strains and bending curvatures as shown in Eq. (4):

$$\epsilon = \begin{Bmatrix}\epsilon^o\\ \kappa\end{Bmatrix} = \begin{bmatrix}\epsilon_{11}\\ \epsilon_{22}\\ \epsilon_{12}\\ \kappa_{11}\\ \kappa_{22}\\ \kappa_{12}\end{bmatrix} = \begin{Bmatrix} \dfrac{\partial u}{\partial x}\\ \dfrac{\partial v}{\partial y}\\ \dfrac{1}{2}\left(\dfrac{\partial u}{\partial y} + \dfrac{\partial v}{\partial x}\right)\\ -\left(\dfrac{\partial^2 w}{\partial x^2}\right)\\ -\left(\dfrac{\partial^2 w}{\partial y^2}\right)\\ -\left(\dfrac{\partial^2 w}{\partial x\partial y}\right)\end{Bmatrix} \tag{4}$$

The laminate and actuator stiffness matrices are composed of the reduced stiffnesses of each ply in the laminate axes. Equation (5) shows the equilibrium condition of an active laminate that is moved by actuator elements without external forces:

$$\begin{bmatrix}A & B\\ B & D\end{bmatrix}_l\begin{Bmatrix}\epsilon^o\\ \kappa\end{Bmatrix} = \begin{Bmatrix}N\\ M\end{Bmatrix}_a = \begin{bmatrix}A & B\\ B & D\end{bmatrix}_a\begin{Bmatrix}\Lambda_\epsilon\\ \Lambda_\kappa\end{Bmatrix} \tag{5}$$

Since CAP elements have been the most commonly used piezoelectric actuators, they will be contrasted to DAP actuators which are artifically orthotropic. CAP elements are fundamentally isotropic and produce roughly equal in-plane strains. For analysis, the strains will be assumed to be equal, although for many types of piezoceramics there are slight differences between d_{31} and d_{32}. DAP elements can also be modeled as having equal in-plane strains. However, from the directional attachment, their stiffnesses in the longitudinal and lateral directions will differ greatly. Equation (6) shows the strain actuation vector available from CAP elements:

$$\begin{bmatrix}A & B\\ B & D\end{bmatrix}_a\begin{Bmatrix}\Lambda_\epsilon\\ \Lambda_\kappa\end{Bmatrix} = \begin{bmatrix}A & B\\ B & D\end{bmatrix}_a\begin{Bmatrix}\Lambda_\epsilon\\ 0\end{Bmatrix} = \begin{Bmatrix}(A_{11}+A_{12})\Lambda\\ (A_{11}+A_{12})\Lambda\\ 0\\ (B_{11}+B_{12})\Lambda\\ (B_{11}+B_{12})\Lambda\\ 0\end{Bmatrix}_a \tag{6}$$

The zeroes in the shear and twist generation terms in Eq. (6) point out that the CAP actuators can only produce twist in coupled lamina. DAP elements, however, have a fully populated actuation vector as shown in Eq. (7):

$$\begin{bmatrix} A & B \\ B & D \end{bmatrix}_a \begin{Bmatrix} \Lambda_\epsilon \\ \Lambda_\kappa \end{Bmatrix} = \begin{bmatrix} A & B \\ B & D \end{bmatrix}_a \begin{Bmatrix} \Lambda_\epsilon \\ 0 \end{Bmatrix} = \begin{Bmatrix} (A_{11} + A_{12})\Lambda \\ (A_{12} + A_{22})\Lambda \\ (A_{16} + A_{26})\Lambda \\ (B_{11} + B_{12})\Lambda \\ (B_{12} + B_{22})\Lambda \\ (B_{16} + B_{26})\Lambda \end{Bmatrix}_a \tag{7}$$

As a result, DAP elements can produce any possible laminate deflection, including extension, shear, bending, and twist. Further, because the DAP plies can be arranged to cancel some strains, it is now possible to use DAP elements to completely decouple active strains. That is, the DAP plies may generate pure twist without inadvertently exciting bending or extensional deflections.

Analysis of a Symmetric Two-DAP Ply Laminate

Many structures require torsional vibration control without cross-feed of active deflections to extensional modes. The simplest method of accomplishing this is to use a three-ply laminate with symmetrically laminated DAP elements: [+ΘDAP/uncoupled substrate/ + ΘDAP]. This arrangement decouples the extensional and twist modes of the laminate and through the stiffness of the DAP elements lends a slight bending-twist coupling.

If the top and bottom DAP elements are actuated in opposite directions [+ ΘDAP(+ Λ)/uncoupled substrate/ + ΘDAP(− Λ)], then the laminate will bend and twist. As a result, Eq. (5) reduces to a pair of 3 × 3 matrices as seen in Eq. (8):

$$\begin{bmatrix} B_{11} & B_{12} & 2B_{16} \\ B_{12} & B_{22} & 2B_{26} \\ B_{16} & B_{26} & 2B_{66} \end{bmatrix}_a \begin{bmatrix} \Lambda \\ \Lambda \\ 0 \end{bmatrix}_a = \begin{bmatrix} D_{11} & D_{12} & 2D_{16} \\ D_{12} & D_{22} & 2D_{26} \\ D_{16} & D_{26} & 2D_{66} \end{bmatrix}_l \begin{bmatrix} \kappa_{11} \\ \kappa_{22} \\ \kappa_{12} \end{bmatrix}_l \tag{8}$$

If the laminate is free on all edges, with no externally applied forces, then the laminate twist can be expressed as Eq. (9):

$$\kappa_{12} = \frac{(D_{11}D_{22} - D_{12}^2)_l(B_{16} + B_{26})_a + (D_{12}D_{26} - D_{22}D_{16})_l(B_{11} + B_{12})_a + (D_{12}D_{16} - D_{11}D_{26})_l(B_{22} + B_{12})_a}{2[(D_{11}D_{22} - D_{12}^2)_l D_{66l} + (D_{12}D_{26} - D_{22}D_{16})_l D_{16l} + (D_{12}D_{16} - D_{11}D_{26})_l D_{26l}]}\Lambda \tag{9}$$

It can be easily shown that the twist deflection of this laminate is increased if it is constrained longitudinally and laterally and the elements are oriented at 45 deg. If the laminate is prevented from bending in the longitudinal and lateral directions to increase the twist deflections, then Eq. (9) reduces to a very simple form as shown in Eq. (10).

$$\kappa_{12} = \frac{(E_L - E_T)(t_s t_a + t_a^2)}{(E_s t_s/6)[(1 - \nu_{LT}\nu_{TL})/(1 + \nu_s)] + (E_L + E_T - 2E_T\nu_{LT})[(t_s^2 t_a/2) + t_s t_a^2 + (2t_a^3/3)]}\Lambda \tag{10}$$

Torque plates of this type may be used in many different structures, including active wings and rotor blades. Although laminate constraint would significantly enhance wing and rotor deflections, the associated external structure may prove too cumbersome for many other applications. Accordingly, an antisymmetric laminate should be investigated to reduce the actuator size.

Analysis of an Antisymmetric Two-DAP Ply Laminate

Antisymmetric torque plates effectively decouple the bending and twist terms. The simplest form of antisymmetric DAP laminate is constructed as [+ ΘDAP/uncoupled substrate/ − ΘDAP]. When the plies are actuated in the same direction, the laminate extends in two directions and twists. Equation (5) degenerates to a pair of 3 × 3 matrices as shown in Eq. (11):

$$\begin{bmatrix} A_{11} & A_{12} & 2B_{16} \\ A_{12} & A_{22} & 2B_{26} \\ B_{16} & B_{26} & 2D_{66} \end{bmatrix}_a \begin{bmatrix} \Lambda \\ \Lambda \\ 0 \end{bmatrix}_a = \begin{bmatrix} A_{11} & A_{12} & 2B_{16} \\ A_{12} & A_{22} & 2B_{26} \\ B_{16} & B_{26} & 2D_{66} \end{bmatrix}_l \begin{bmatrix} \epsilon_{11} \\ \epsilon_{22} \\ \kappa_{12} \end{bmatrix}_l \tag{11}$$

Constraint of the antisymmetric DAP laminate in the extensional modes will generally increase the amount of twist deflection. Unfortunately, extensional constraint is not as easy as with bending constraints, so a stiff substrate should be used to maximize twist deflections. Beryllium is among the best materials; however, steel substrates are adequate as their stiffness is high and they are more easily machined than beryllium.

Since the constraint of the antisymmetric DAP laminate is very difficult, Eq. (11) can be expanded to show the major terms of the unconstrained twisting laminate:

$$\kappa_{12} = \frac{[(A_{11}A_{22} - A_{12}^2)_l(B_{16} + B_{26})_a + (A_{12}B_{26} - A_{22}B_{16})_l(A_{11} + A_{12})_a + (A_{12}B_{16} - A_{11}B_{26})_l(A_{22} + A_{12})_a]}{2[(A_{11}A_{22} - A_{12}^2)_l D_{66l} + (A_{12}B_{26} - A_{22}B_{16})_l B_{16l} + (A_{12}B_{16} - A_{11}B_{26})_l B_{26l}]}\Lambda \tag{12}$$

If the DAP elements are oriented at ±45 deg to produce maximum deflections, and it is assumed that the denominators of the reduced stiffnesses are approximately equal ($1 - \nu_{LTa}\nu_{TLa} \cong 1 - \nu_s^2$), then Eq. (12) reduces to Eq. (13):

$$\kappa_{12} = \frac{[E_s t_s(1 + \nu)](E_{Ta} - E_{La})(t_s t_a + t_a^2)\Lambda}{\left([E_s t_s(1 + \nu) + (E_{La} + E_{Ta} + 2E_{La}\nu_{TL})t_a]\{E_s t_s^3(1 - \nu)/6 + (E_{La} + E_{Ta} - 2E_{La}\nu_{TL})[(t_s^2 t_a/2) + t_s t_a^2 + (2t_a^3/3)]\} - \tfrac{1}{2}[(t_s t_a + t_a^2)(E_{La} - E_{Ta})]^2\right)} \tag{13}$$

The assumption that the denominators of the reduced stiffnesses are approximately equal will induce slight errors up to 5%. Equation (13) can be further modified to account for finite thickness bonds by modifying the substrate stiffness and thickness. In general, differences generated by bond thicknesses will be negligible as long as the bond thickness is an order of magnitude smaller than the actuator element and the substrate.

Decoupling of Active Strains and Curvatures

For many structural control systems, a complete decoupling of actuation strains is required so that energy from one mode of control is not fed to another. For instance, control of plate twist modes often excites transverse bending or extension modes if not completely decoupled. DAP and CAP elements may be used to achieve this decoupling with a ply sequence of (DAP/CAP/uncoupled substrate/CAP/DAP). The DAP and CAP ply actuation sequence is shown in Table 1 for generating any desired plate strain or curvature. The CAP balancing strains λ are primarily used to remove the secondary strains. If the CAP and DAP elements are made of the same actuator material, and the directional attachment is ideal, such that the orthotropy ratio $OR = \infty$, then the balancing strains may be solved for as shown in Eqs. (14–19):

$$\lambda_{\epsilon 11sy} = \lambda_{\epsilon 22sy} = \lambda_{\epsilon 11an} = \lambda_{\epsilon 22an} = \frac{\nu t_D(2E_a t_C + E_s t_s)}{t_C[2(1+\nu)E_a t_D + 2E_a t_C + E_s t_s]}\Lambda \tag{14}$$

$$\lambda_{\epsilon 12sy} = \frac{t_D(\nu - 1)(E_a t_C + \tfrac{1}{2}E_s t_s)}{t_C[(1+\nu)E_a t_D + 2E_a t_C + E_s t_s]}\Lambda \tag{15}$$

$$\lambda_{\epsilon 12an} = \frac{[(t_s + 2t_C)t_D + t_D^2](\nu - 1)(E_a t_C + \tfrac{1}{2}E_s t_s)}{(t_s t_C + t_C^2)[(1+\nu)E_a t_D + 2E_a t_C + E_s t_s]}\Lambda \tag{16}$$

$$\lambda_{\kappa 11sy} = \lambda_{\kappa 22sy} = \lambda_{\kappa 11an} = \lambda_{\kappa 22an}$$

$$= \frac{\nu[(t_s + 2t_C)t_D + t_D^2]\{E_a[(t_s^2 t_c/2) + t_s t_C^2 + (2t_C^3/3)] + (E_s t_s^3/12)\}}{(t_s t_C + t_C^2)\left((1+\nu)E_a\{[(t_s + 2t_C)^2 t_D/2] + (t_s + 2t_C)t_D^2 + (2t_D^3/3)\} + E_a[(t_s^2 t_c/2) + t_s t_C^2 + (2t_C^3/3)] + (E_s t_s^3/12)\right)}\Lambda \tag{17}$$

$$\lambda_{\kappa 12an}$$

$$= \frac{[(t_s + 2t_C)t_D + t_D^2](\nu - 1)\{(E_a/2)[(t_s^2 t_c/2) + t_s t_C^2 + (2t_C^3/3)] + (E_s t_s^3/24)]\}}{(t_s t_C + t_C^2)\left((1+\nu)(E_a/2)\{[(t_s + 2t_C)^2 t_D/2] + (t_s + 2t_C)t_D^2 + (2t_D^3/3)\} + E_a[(t_s^2 t_c/2) + t_s t_C^2 + (2t_C^3/3)] + (E_s t_s^3/12)\right)}\Lambda \tag{18}$$

$$\lambda_{\kappa 12an}$$

$$= \frac{(E_a/2)[(t_s + 2t_C)t_D + t_D^2]^2(1+\nu) - \left(E_a(1+\nu)\{[(t_s + 2t_C)^2 t_D/2] + (t_s + 2t_c)t_D^2 + (2t_D^3/3)\} + 2E_a[(t_s^2 t_C/2) + t_s t_C^2 + (2t_C^3/3)] + (E_s t_s^3/6)\right)t_D}{[2t_C/(1-\nu)]\left(E_a(1+\nu)\{[(t_s + 2t_C)^2 t_D/2] + (t_s + 2t_C)t_D^2 + (2t_D^3/3)\} + 2E_a[(t_s^2 t_c/2) + t_s t_C^2 + (2t_C^3/3)] + (E_s t_s^3/6)\right)}\Lambda \tag{19}$$

(The assumption of ideal directional attachment is acceptable for many advanced attachment patterns as orthotropy ratios in excess of 50 are common.)

Experimental DAP Specimens

Two different specimens were constructed to demonstrate the principle of directional attachment. The first specimens were constructed from beam elements to verify the theory. The second specimen was a torque-plate wing that used DAP elements to induce pitch deflections.

Aluminum-DAP Beam Specimens

Two plate specimens were constructed to demonstrate the concept of directional attachment. The first beam was constructed from 0.030-in. (0.0762-cm) thick 2024-T3 aluminum with DAP elements laid up at 0 and 90 deg as shown in Fig. 5. They were bonded to the aluminum beams with Hexcel Safe-T-Poxy™ in a room temperature cure with electrical leads taken off the bottom and tops of the elements along the longitudinal center-lines. The DAP elements were cut from 0.0075-in. (0.01905-cm) thick G-1195 PZT with nickel faces. Two parting areas were masked off by the presence of a 1-mil-thick layer of Teflon sheet between the beam and the DAP elements. This parting strip was removed after the cure to leave the elements free in the lateral directions. A second beam specimen was used to test the twist generation capability of DAP elements. As shown in Fig. 6, the elements were arranged antisymmetrically at 45 deg on either side of a 0.030-in. (0.0762-cm) 2024-T3 aluminum beam. Direct current (dc) signals were sent to the beam, and the deflections were measured by reflecting a laser off a mirror mounted on the end of the beam.

DAP Torque-Plate Wing Specimen

The DAP torque-plate wing was constructed from an active plate mounted inside a subsonic missile fin shell with an aspect

Table 1 Order of DAP and CAP ply actuation for generating decoupled strains and curvatures

Desired strain or curvature	DAP ply 1	CAP ply 1	CAP ply 2	DAP ply 2
	Symmetric DPA Piles			
ϵ_{11}	0 deg, $+\Lambda$	$+\lambda_{\epsilon 11sy}$	$+\lambda_{\epsilon 11sy}$	0 deg, $+\Lambda$
ϵ_{22}	+90 deg, $+\Lambda$	$+\lambda_{\epsilon 22sy}$	$+\lambda_{\epsilon 22sy}$	+90 deg, $+\Lambda$
ϵ_{12}	+45 deg, $+\Lambda$	$-\lambda_{\epsilon 12sy}$	$-\lambda_{\epsilon 12sy}$	+45 deg, $+\Lambda$
κ_{11}	0 deg, $+\Lambda$	$+\lambda_{\kappa 11sy}$	$-\lambda_{\kappa 11sy}$	0 deg, $-\Lambda$
κ_{22}	+90 deg, $+\Lambda$	$+\lambda_{\kappa 22sy}$	$-\lambda_{\kappa 22sy}$	+90 deg, $-\Lambda$
κ_{12}	+45 deg, $+\Lambda$	$-\lambda_{\kappa 12sy}$	$+\lambda_{\kappa 12sy}$	+45 deg, $-\Lambda$
	Antisymmetric DPA Piles			
ϵ_{11}	0 deg, $+\Lambda$	$+\lambda_{\epsilon 11an}$	$+\lambda_{\epsilon 11an}$	0 deg, $+\Lambda$
ϵ_{22}	+90 deg, $+\Lambda$	$+\lambda_{\epsilon 22an}$	$+\lambda_{\epsilon 22an}$	−90 deg, $+\Lambda$
ϵ_{12}	+45 deg, $+\Lambda$	$-\lambda_{\epsilon 12an}$	$+\lambda_{\epsilon 12an}$	−45 deg, $-\Lambda$
κ_{11}	0 deg, $+\Lambda$	$+\lambda_{\kappa 11an}$	$-\lambda_{\kappa 11an}$	0 deg, $-\Lambda$
κ_{22}	+90 deg, $+\Lambda$	$+\lambda_{\kappa 22an}$	$-\lambda_{\kappa 22an}$	−90 deg, $-\Lambda$
κ_{12}	+45 deg, $+\Lambda$	$-\lambda_{\kappa 12an}$	$-\lambda_{\kappa 12an}$	−45 deg, $+\Lambda$

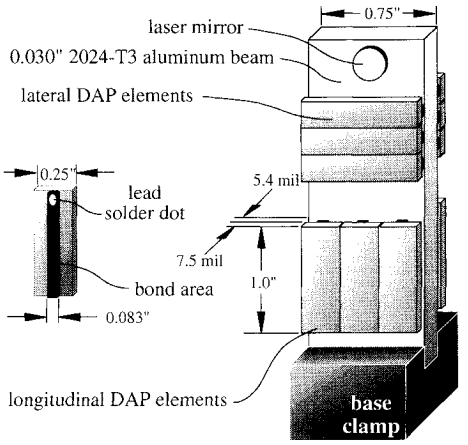

Fig. 5 Longitudinal and lateral DAP beam.

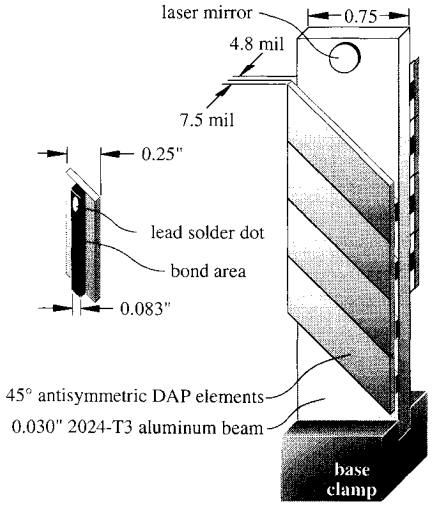

Fig. 6 Antisymmetric DAP beam.

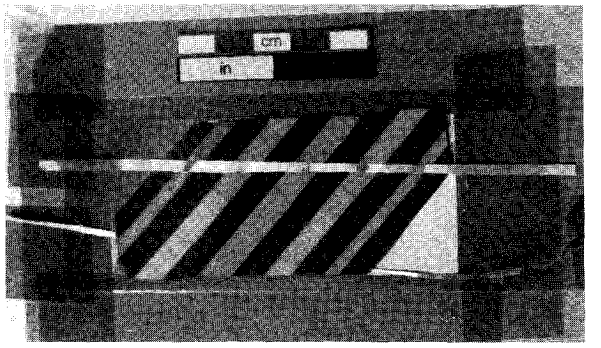

Fig. 7 DAP elements before bonding on torque plate.

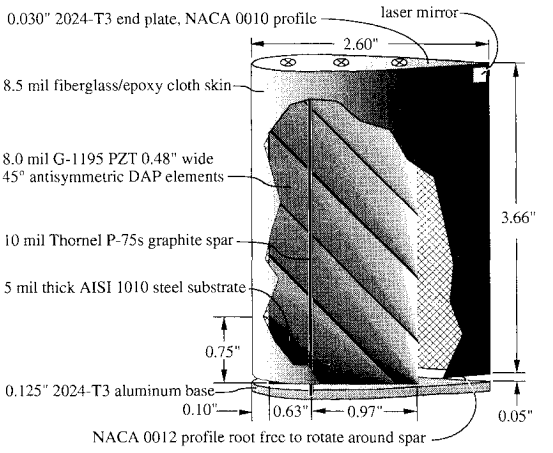

Fig. 8 NACA 0012 DAP torque-plate wing structure.

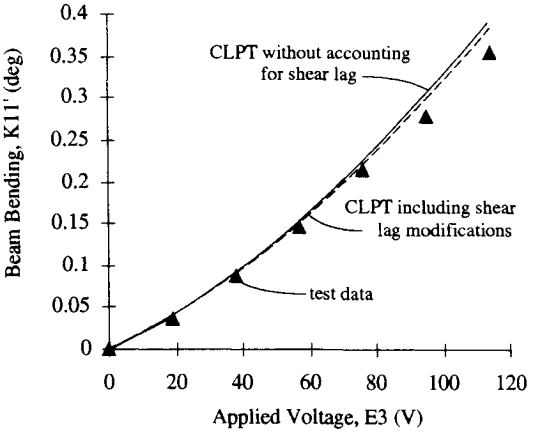

Fig. 9 Beam bending due to longitudinally attached DAP elements.

ratio of 1.4. The torque plate was bonded at the wing root to a fixed base and to the shell at the wing tip. The wing skin had NACA 0010 and 0012 profiles at the tip and root. The torque plate was strengthened in bending by a pair of Thornel P75™ graphite strips that were arranged as a main spar.

The DAP torque plate was constructed of 10 DAP elements mounted on a 5-mil-thick AISI 1010 steel plate. The 8-mil-thick lead zirconate titanate DAP elements were bonded to the surface of the plate with Hexcel Safe-T-Poxy in a room temperature cure forming a nominal 5-mil-thick bond. One-mil-thick siliconized tape was used for the parting ply as seen in Fig. 7 mounted on the top side of the DAP elements. The tape on the top side of the elements was rectangular in shape and functioned as jigging so as to maintain tolerances during the cure process. The upper layer of tape was sealed against the

Table 2 Stiffness and thickness of DAP beam components

	E_{Lo}, Msi	E_{To}	G_{LTo}	E_{Leffo}	E_{Teffo}	G_{effo}	E_{Leff}	E_{Teff}	G_{eff}	t, mil
Longitudinal and lateral DAP beam										
DAP longitudinal	9.14	9.14	3.44	8.63	3.05	3.25	8.05	1.65	3.03	7.5
DAP lateral	9.14	9.14	3.44	8.46	3.05	3.18	7.70	1.65	2.90	7.5
Bond	0.421	0.421	0.160	—	—	—	—	—	—	5.4
Substrate	10.1	10.1	3.81	—	—	—	—	—	—	30.0
Torsion DAP beam										
DAP longitudinal	9.14	9.14	3.44	8.66	3.05	3.25	8.15	1.67	3.06	7.5
Bond	0.421	0.421	0.160	—	—	—	—	—	—	4.8
Substrate	10.1	10.1	3.81	—	—	—	—	—	—	30.0

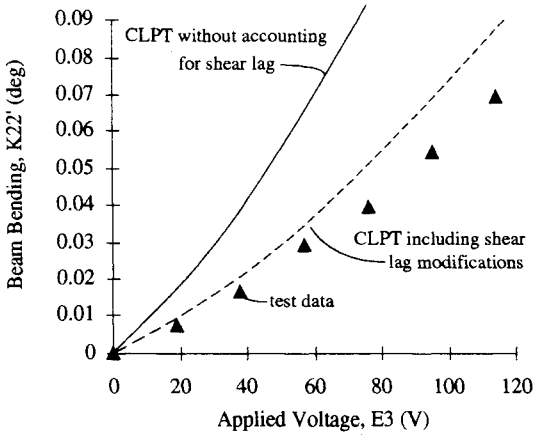

Fig. 10 Beam bending due to laterally attached DAP elements.

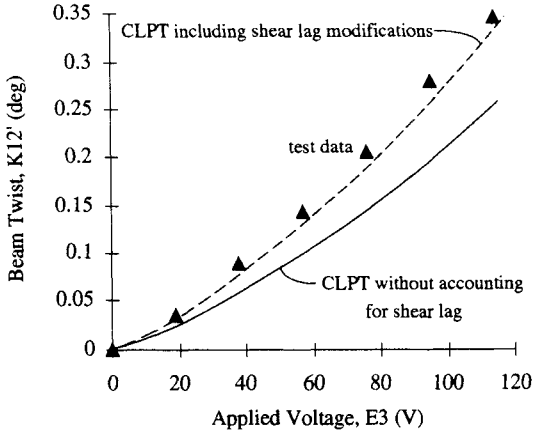

Fig. 11 Beam twist due to 45-deg antisymmetric DAP elements.

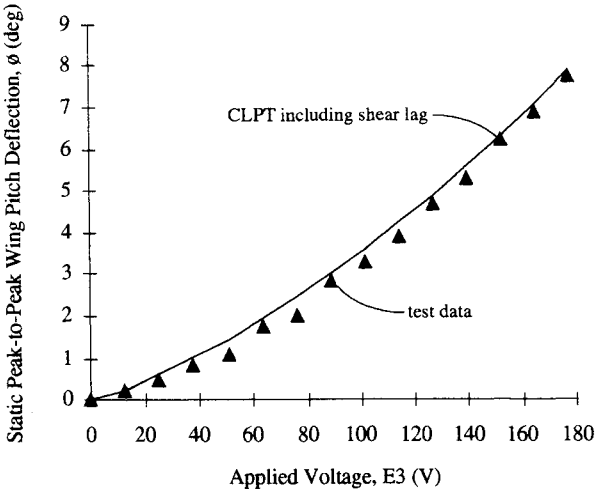

Fig. 12 DAP torque-plate wing static deflecition.

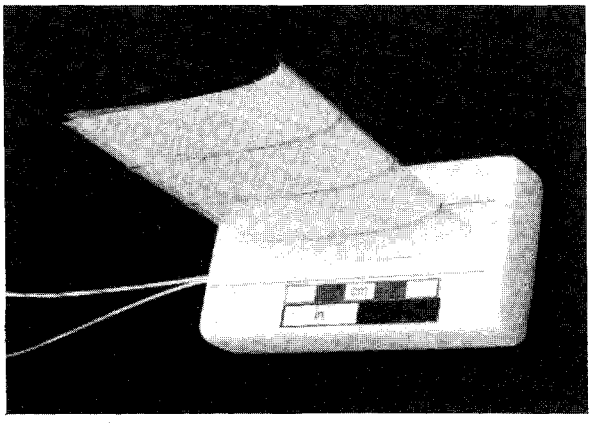

Fig. 13 DAP wing undergoing ±2-deg static deflections at ±90 V (one-half of maximum deflection).

bottom to retarded resin creep from the open ends of the DAP elements, which destroys DAP element orthotropy.[9]

The DAP elements were soldered in parallel with 1-mil-thick brass foil strips as seen in Fig. 7. The bottom foil strips were grounded to the torque plate. The schematic of the DAP elements, torque plate, skin, and base mount is shown in Fig. 8.

The root of the torque plate was fixed in a rigid aluminum base. The tip of the torque plate was rigidly fixed to the inside of the end of the wing as shown in Fig. 8 by an end plate that was bonded to the torque plate and fastened to the end of the wing skin. A graphite stiffener was constructed from Thornel P-75s uniaxial fibers and Hexcel Safe-T-Poxy bonded in a room temperature cure. The stiffener was placed just ahead of the aerodynamic center of the wing at the 24% chord. The elastic axis was accordingly positioned on the quarter-chord, so that no degradation in pitch deflections would occur with increasing angle of attack (below the stall). For aeroservoelastic applications, the location of the stiffener will be moved further back so that air loads may be used to help pitch the wing. The wing mass without the end plate and base mount was 25.2 g (0.89 oz).

Beam and Torque-Plate Wing Test Results

Plate Specimens

The bending deflections of the plate specimen in Fig. 5 were estimated by calculating the effective stiffnesses of the DAP elements and substituting those effective stiffnesses into Eq. (5). The twist estimation for the antisymmetric specimen of Fig. 6 was made similarly. The values for the effective stiff-

nesses are as shown in Table 2 for the three different DAP test arrangements.

Figures 9–11 show the bending and twist deflections generated by the DAP beam specimens. The stiffness estimations of Table 2 (from the DAP effective stiffness models) were used in the CLPT predictions shown in Figs. 9–11. These models show good correlation with experiment. It is thought that the errors are primarily due to inaccuracies in measuring the amount of directional attachment. Other sources of inaccuracies may be the inconsistency in bondline thickness along the length of the elements. The variation in bondline thickness was held to less than 0.5 mil. Still, this variation may have been enough to cause deviations in theory and experiment. The values for the bondline thicknesses shown in Table 2 are the average values of all of the elements that were directionally attached to the aluminum substrates.

From Fig. 9, the longitudinal strain reduction due to shear lag is very small. Shear lag modifications in effective stiffness taken into account through Eq. (3) have little impact on the final results. In the lateral direction, however, the inclusion of shear lag is very important as shown in Fig. 10. The inaccuracy of using only partial attachment estimations demonstrates that the effective stiffness must be modified by shear lag estimations to be accurate. For longitudinal bending, the difference between theory and experiment is less than 7%. The error increases in the lateral case to over 25%. Transverse microcracking and a nonuniform bond thickness may have contributed to the large difference between theory and experiment. It should be noted that the transverse estimation is not nearly as critical as the longitudinal estimations since most structural actuation is performed in the longitudinal direction. The longitudinal strain generated by the antisymmetrically laminated elements produced twist deflections in excess of 0.3 deg and a difference between theory and experiment of less than 4.5%.

Wing Specimen Test Results

As with the DAP beam specimens, estimations of the element effective stiffnesses were made, then integrated into Eq. (13) for twist estimation. The graphite spar shown in Fig. 8 increased the torsional stiffness of the laminate by approximately 4%. This addition in passive torsional stiffness was accounted for in the laminated plate theory model of Eq. (5). Figure 12 shows that the DAP torque plate was energized to more than 170 V dc. At this high potential, deflections in excess of 8 deg peak-to-peak were generated. The wing showed no frictional effects during testing as there were no hinges, linkages, or push rods. Hysteresis and creep typical of the G1195-PZT were experienced. All 10 elements maintained proper poling, and end arcing was imperceptible. Figure 13 shows the torque-plate wing undergoing ± 2-deg deflections at 90-V actuation potential.

Dynamic testing of the wing was also performed. The wing was energized at 119 V ac from 0.1 to 100 Hz with a sinusoidal signal. Figure 14 shows the frequency response of the wing, demonstrating a break frequency in excess of 80 Hz. During dynamic testing, the participation of the first bending mode in the shell was present from 55–70 Hz, which was due to the large mass of the end plate at the tip of the wing. The maximum eccentricity of the resulting Lissajous figure traced by the reflected laser beam was less than 4.5%.

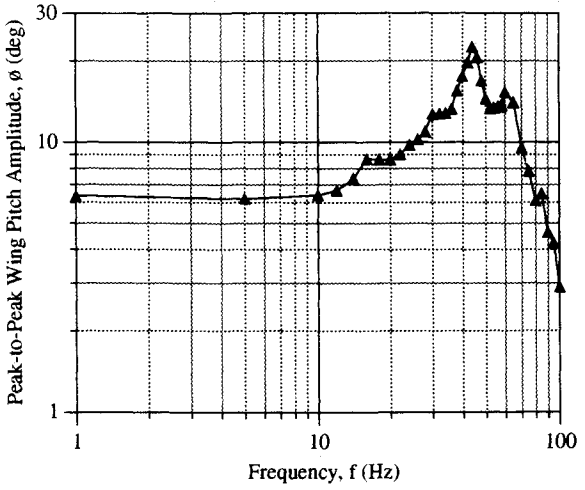

Fig. 14 DAP wing frequency response at 122 V ac.

Conclusions

It can be concluded that there are three ways of achieving directional attachment: 1) partial attachment, 2) transverse shear lag, and 3) differential stiffness bonding. Estimation of DAP laminate strains are accomplished by 1) determining the reductions in longitudinal and lateral effective stiffnesses caused by each of the three attachment methods, and then 2) substituting these effective moduli in laminated plate theory stiffness terms to determine the laminate strains.

Aluminum beams constructed with DAP elements displayed bending rates of 0.36 deg/in. (14 deg/m) and twist rates of 0.23 deg/in. (9 deg/m). Analytical models based on laminated plate theory showed good correlation with experimental data. The longitudinal bending rate estimations differed from experiment by 7%, and the twist rate models differed by less than 4.5%. The lateral bending rate estimation differed from experiment by 25%.

The plate models showed that lamina could be constructed with DAP and CAP elements so that pure strains—ϵ_{11}, or ϵ_{22}, or ϵ_{12}, and pure curvatures—κ_{11}, or κ_{22}, or κ_{12}—could be generated without cross-feeding to any other strain or curvature. For complete decoupling of the strains and curvatures, a 5-ply laminate must be constructed with an uncoupled substrate with an arrangement of [DAP/CAP/uncoupled substrate/CAP/DAP].

A torque-plate wing using antisymmetrically laminated DAP elements and a graphite spar induced static pitch deflections in excess of 8 deg peak-to-peak. The wing demonstrated a break frequency in excess of 80 Hz and was designed to maintain constant deflections with increasing airspeed up to Mach 0.7.

Acknowledgments

The author wishes to express his sincere appreciation to the University of Kansas Aerospace Engineering Department and the Kansas Space Grant Consortium, funded by NASA Headquarters, for providing him with support.

References

[1]Crawley, E. F., and Anderson, E. H., "Detailed Models of Piezoceramic Actuation of Beams," *Proceedings of the AIAA/ASME/ASCE/AHS 30th Structures, Structural Dynamics, and Materials Conference* (Mobile, AL), AIAA, Washington, DC, 1989, pp. 2000–2010 (AIAA Paper 89-1388).

[2]Anderson, E. H., "Piezoceramic Induced Strain Actuation of One- and Two-Dimensional Structures," S.M. Thesis, Dept. of Aeronautics and Astronautics, Massachusetts Inst. of Technology, Cambridge, MA, 1989.

[3]Hanagud, S., Obal, M. W., and Claise, A. J., "Optimal Vibration Control by the Use of Piezoceramic Sensors and Actuators," *Proceedings of the AIAA/ASME/ASCE/AHS 28th Structures, Structural Dynamics, and Materials Conference,* AIAA, New York, 1987, pp. 987–997.

[4]Crawley, E. F., and De Luis, J., "Use of Piezoelectric Actuators as Elements of Intelligent Structures," *AIAA Journal,* Vol. 25, No. 10, 1987, pp. 1373–1385.

[5]Sung, C. C., Varadan, V. V., Bao, X. Q., and Varadan, V. K., "Active Control of Torsional Vibration Using Piezoceramic Sensors and Actuators," *Proceedings of the AIAA/ASME/ASCE/AHS 31st Structures, Structural Dynamics, and Materials Conference* (Long Beach, CA), AIAA, Washington, DC, 1990, pp. 2317–2322 (AIAA

Paper 90-1130).

[6]Lee, C. K., "Piezoelectric Laminates for Torsional and Bending Modal Control: Theory and Experiment," Ph.D. Thesis, Dept. of Applied Mechanics, Cornell Univ., Ithaca, NY, 1987.

[7]Crawley, E. F., and Lazarus, K. B., "Induced Strain Actuation of Isotropic and Anisotropic Plates," *AIAA Journal,* Vol. 29, No. 6, 1991, pp. 944–951.

[8]Crawley, E. F., Lazarus, K. B., and Warkentin, D. J., "Embedded Actuation and Processing in Intelligent Materials," *Compendium from the 2nd International Workshop on Composite Materials and Structures for Rotorcraft* (Troy, NY), American Helicopter Society, Alexandria, VA, 1989.

[9]Barrett, R. M., "Intelligent Rotor Blade and Structural Development Using Directionally Attached Piezoelectric Crystals," M.S. Thesis, Aerospace Engineering Dept., Univ. of Maryland, College Park, MD, May 1990.

[10]Barrett, R. M., "Intelligent Rotor Blade Actuation Through Directionally Attached Piezoelectric Crystals," Lichten Competition Finalist Paper, American Helicopter Society National Forum, Washington, DC, May 1990.

[11]Barrett, R. M., "Method and Apparatus for Structural Actuation and Sensing in a Desired Direction," U.S. Patent Application 485,599, Feb. 1990.

[12]Barrett, R. M., "Actuation Strain Decoupling Through Enhanced Directional Attachment in Plates and Aerodynamic Surfaces," *Proceedings of the 1st European Conference on Smart Structures and Materials* (Glasgow, Scotland), IOP Publishing, Bristol, England, UK, 1992, pp. 383–386.

[13]Chen, P. C., Samak, D. K., and Chopra, I., "Development of an Intelligent Rotor," *Proceedings of the 4th Workshop on Dynamics and Aeroelastic Stability Modeling of Rotorcraft Systems,* Univ. of Maryland, College Park, MD, Nov. 1991.

[14]Nitzsche, F., and Breitbach, E., "A Study on the Feasibility of Using Adaptive Structures in the Attenuation of Vibration Characteristics of Rotary Wings" *Proceedings of the AIAA/ASME/ASCE/AHS 33rd Structures, Structural Dynamics, and Materials Conference* (Dallas, TX), AIAA, Washington, DC, 1992, pp. 1391–1402 (AIAA Paper 92-2452).

[15]Jones, R. M., *Mechanics of Composite Materials,* Hemisphere, New York, 1975, pp. 147–237.